Available online at www.sciencedirect.com
ScienceDirect
Solid State Communications 143 (2007) 20–26
solid state communications
www.elsevier.com/locate/ssc

The quantum Hall effect in graphene from a lattice perspective

B. Andrei Bernevig[a,b], Taylor L. Hughes[a,*], Shou-Cheng Zhang[a]

[a] *Department of Physics, Stanford University, Stanford, CA 94305, United States*
[b] *Princeton Center for Theoretical Physics, Princeton University, Princeton, NJ 08544, United States*

Accepted 18 April 2007 by A.H. MacDonald
Available online 29 April 2007

Abstract

The recent quantum Hall experiments in graphene have confirmed the theoretically well-understood picture of the quantum Hall conductance in fermion systems with continuum Dirac spectrum. In this paper we take into account the lattice, and perform an exact diagonalization of the Landau problem on the hexagonal lattice. At very large magnetic fields the continuum Dirac argument fails completely and the Hall conductance, given by the number of edge states present in the bulk gaps of the spectrum, is dominated by lattice effects. As the field is lowered, the experimentally observed situation is recovered through a phenomenon which we call band collapse. As a corollary, for low magnetic field, graphene will exhibit two qualitatively different quantum Hall effects (QHEs): at low filling, the QHE will be dominated by the "relativistic" Dirac spectrum and the Hall conductance will be odd-integer; above a certain filling, the QHE will be dominated by a non-relativistic spectrum, and the Hall conductance will span all integers, even and odd.

PACS: 73.43.-f; 71.10.Fd; 71.10.Pm; 71.70.Di

Keywords: A. Graphene; D. Quantum Hall effect; D. Edge states

The recent explosion of research on graphene stems from the successful production and measurement of two-dimensional planar sheets of graphite by two separate groups [1,2]. These two groups confirm an interesting behavior of the quantum Hall effect (QHE) in graphene in which the transverse conductance is quantized as an integer plus a half-integer $\sigma_{xy} = (n + \frac{1}{2})4e^2/h$, where band and spin degeneracies have been taken into account. The unusual phenomenon can be explained by the existence of low-energy Dirac-like spectra at two inequivalent points in the Brilloiun Zone, and although it is unrelated to the parity anomaly, this behavior of the Hall conductance was in fact obvious in the seminal work of Jackiw and Rebbi [3]. On the basis of the continuum argument for the relativistic quantum Hall effect (RQHE) [4–6] the experimental groups conclude that this is an interesting new phenomena completely explained by the relativistic Dirac spectrum of graphene.

We want to improve on this argument for several reasons. For very large B the lattice is expected to dominate the behavior of the Hall conductance. In this regime the Dirac model cannot be valid, since, by virtue of being a continuum argument, it ignores lattice effects and the torus structure of the Brillouin zone. We will see that this is indeed the case, and the large-B limit does not match the Dirac argument prediction. In the experimental situation the magnetic field is weak (with respect to the unit quantum flux per plaquette) and the Dirac argument gives the right result but the use of the Dirac model to classify the Hall conductance for any periodic system is in general inconsistent and only gives correct results for the change in Hall conductance across a gap-closing transition [7]. It works without fault in graphene because of the presence of an even number of Dirac cones. Thus, it is desirable to have a description of the QHE valid for both strong and weak magnetic fields. Using the lattice picture we show how graphene evolves from a high-B regime with non-Dirac behavior to a low-B regime with Dirac behavior through a phenomenon we dub "band collapse". Two adjacent bands close the gap between them across the whole Brillouin zone and form a new band with twice the degeneracy of each of the initial bands. The edge structure reflects this degeneracy.

* Corresponding author.
E-mail address: hughest@stanford.edu (T.L. Hughes).

0038-1098/$ - see front matter © 2007 Elsevier Ltd. All rights reserved.
doi:10.1016/j.ssc.2007.04.031

We begin with a restatement of the RQHE argument based on the relativistic $(2+1)d$ Dirac spectrum. We then present the exact solution of the Landau problem on the graphene lattice. The agreement we find between numerical diagonalization and analytic calculations done with Hatsugai's theoretical transfer matrix framework [8] lead us to our conclusions and illustrate the competition between the relativistic and non-relativistic character of the bandstructure of graphene in a magnetic field.

1. The quantum Hall effect in graphene: Continuum model

We start with the tight-binding nearest-neighbor Hamiltonian for the honeycomb lattice given by Semenoff in Ref. [9]:

$$H = -t\sum_{\vec{A},i} c^\dagger(\vec{A})c(\vec{A}+\vec{b}_i) + c^\dagger(\vec{A}+\vec{b}_i)c(\vec{A}) + \beta\sum_{\vec{A}} c^\dagger(\vec{A})c(\vec{A}) - c^\dagger(\vec{A}+\vec{b}_i)c(\vec{A}+\vec{b}_i) \quad (1)$$

where $c(\vec{A})$, $c(\vec{A}+\vec{b}_i)$ are the annihilation operators for sites on sublattice A and B, and β is an energy difference for electrons localized on the A and B sublattices. We will call this term the Semenoff mass. Graphene is effectively massless which is the limit $\beta \to 0$. In this limit the bandstructure is gapless at two inequivalent points related by time-reversal symmetry $K = \frac{4\pi}{\sqrt{3}a}(\frac{1}{2}, \frac{1}{2\sqrt{3}})$, $K' = -K$, where a is the nearest-neighbor lattice constant. Around these points, the Hamiltonian is described by (in the ideal case massless) Dirac fermions with [9,10]:

$$H_K = \sigma_x k_x + \sigma_y k_y; \qquad H_{K'} = -\sigma_x k_x + \sigma_y k_y \quad (2)$$

which act on a two-spinor wavefunction describing the sublattices A and B, see Fig. 1(a). There is also an overall 2-fold spin degeneracy which we neglect until the final section. Note that parity switches $A \leftrightarrows B$ and $K \leftrightarrows K'$ while time reversal switches $K \leftrightarrows K'$. The Semenoff term opens a gap of value $m = 2\beta/\sqrt{3}ta$ at K and $-m$ at $K' = -K$ so time reversal symmetry is preserved.

Now consider one Dirac fermion at the K-point with mass m in magnetic field B. The Hamiltonian is $H = \sigma_x k_x + \sigma_y(k_y - eBx) + m\sigma_z$. For $eB > 0$, the eigenstates are

$$u^{\pm}_{k,n} = \frac{e^{iky}}{4\pi\alpha_n}\begin{pmatrix} i\sqrt{\alpha_n \pm m}\,\psi_n(x - x_0^{\pm}(k)) \\ \pm\sqrt{\alpha_n \mp m}\,\psi_{n-1}(x - x_0^{\pm}(k)) \end{pmatrix} \quad (3)$$

with

$$\alpha_n = \sqrt{2|eB|n + m^2}$$
$$x_0^{\pm} = \frac{1}{eB}(k \pm \alpha_n)$$
$$E^{\pm} = \pm\alpha_n$$

where $\psi_n(x)$ are harmonic oscillator eigenstates and $u^{\pm}$ are the eigenstates of H_K with energies $E^{\pm}$. Note that all of the energy levels are paired *except* the $n = 0$ level. Observe that for $m > 0$ we have $u^-_{k,0} = 0$ while for $m < 0$ we have $u^+_{k,0} = 0$, so such levels are unpaired even for non-zero mass. In the field theory formalism, the current is defined to be $J^\mu = -\frac{1}{2}e\gamma^\mu_{\beta\alpha}[\psi_\alpha, \overline{\psi}_\beta]$

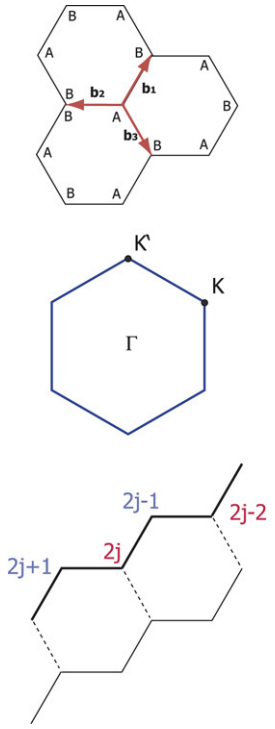

Fig. 1. Graphene lattice, Brilloiun zone and one-dimensional lattice on which Harper's equation is defined.

and is odd with respect to charge conjugation symmetry. We find that

$$\langle 0|J^0|0\rangle = \rho = \frac{1}{2}(N_- - N_+)\frac{|eB|}{2\pi} \quad (4)$$

where N_+ and N_- are the numbers of filled positive and negative energy Landau levels. Hence, the Hall conductance is

$$\sigma_{xy} = \frac{1}{2}(N_- - N_+) \quad (5)$$

in units of e^2/h. Due to the unpaired level, this will be a half-integer and the position of the unpaired level depends on the sign of eB and m. This line of argument follows that of Ref. [11].

This analysis is correct for the fermion located around the K-point, but as mentioned before the graphene bandstructure contains two such fermions. For the purpose of being well defined, we consider a small positive Semenoff mass m at K which means a small negative mass at K'. Consider the case of $eB > 0$. The Hall conductance gets a contribution from both fermions and is zero when the Fermi level is in the gap $-m < \mu < m$ and *odd* integer otherwise. This is then an *odd integer QHE* as in Fig. 2. When the gap is vanishingly small, $m \to 0$, the region of zero Hall conductance becomes infinitely narrow.

2. The quantum Hall effect in graphene: Lattice model

We now present a different argument that reproduces the experimental results and is valid for both high and low B. The solution to this problem is to carefully examine the

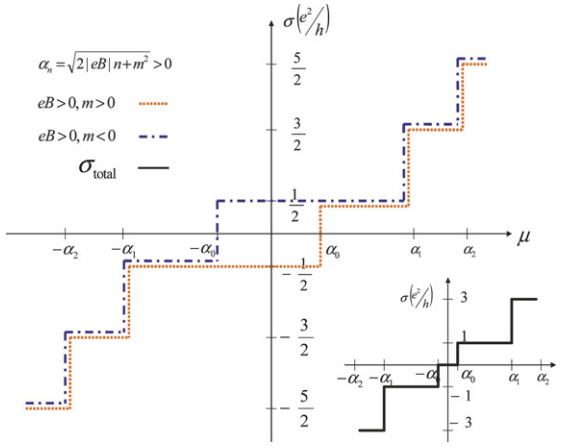

Fig. 2. Hall conductance as a function of the chemical potential. The red and blue are the individual conductances from the two Dirac cones whereas the yellow one is the total Hall conductance. (For interpretation of the references to colour in this figure legend, the reader is referred to the web version of this article.)

bandstructure and edge states of graphene in a magnetic field with rational flux $\phi = p/q$. The analysis is based on a generalization of Hatsugai's analytical transfer matrix method in Ref. [8] to the honeycomb lattice. The energies of the bulk bands and edge states of the system are found as zeros of certain polynomial equations. By using general polynomial theory we are able to characterize the bands, find the number of band crossings, and determine the conditions for zero modes and edge states. By identifying the Hall conductance as the winding index of the edge state around the band gap, we find that, as the magnetic field is decreased, the winding number of the edge states starts taking odd-integer values due to electron bands collapsing in pairs. The theoretical spectrum is obtained, and, in addition, exact diagonalization results are presented to support it. It will be evident from the calculated bandstructure that for large magnetic fields the Dirac argument does not apply because the Hall conductances of bands at low-filling do not form a sequence of odd-integers in this case, as predicted by the relativistic argument.

We use the Landau gauge $A_y = Bx$, $A_x = 0$, with $B = 2\Phi/3\sqrt{3}a^2$, where $\Phi = p/q$ is the flux per plaquette (hexagon) and p, q are relatively prime integers. With a Peierls substitution the effect of the magnetic field is $c_i^\dagger c_j \to c_i^\dagger c_j \exp\int_j^i \vec{A}\mathrm{d}\vec{r}$. In this gauge $k_y = k$ is a good quantum number and the Hamiltonian for each k is

$$H(k) = -t\sum_j c_{k,2j-1}^\dagger c_{k,2j} A_j(k) + c_{k,2j}^\dagger c_{k,2j+1} + h.c. \qquad (6)$$

where

$$A_j(k) = \mathrm{e}^{\mathrm{i}\pi\frac{p}{q}(j-\frac{5}{6})} + \mathrm{e}^{-\mathrm{i}\pi\frac{p}{q}(j-\frac{5}{6})}\mathrm{e}^{\mathrm{i}k}. \qquad (7)$$

Note that we have not included a mass term in our tight-binding Hamiltonian because graphene is essentially massless. Since $A_{j+q} = (-1)^p A_j$ the Hamiltonian is periodic with period $2q$, $(A_{j+2q} = A_j)$ but the energy spectrum, which depends only on $|A_j|$ is periodic with period q. We start with the one-particle states $|\Psi(k,\phi)\rangle = \sum_i \psi_i(k,\phi)c_{k,i}^\dagger|0\rangle$ and act on these with the Hamiltonian to obtain the equation $H|\Psi\rangle = E|\Psi\rangle$. There are two independent amplitude equations, one for i odd and one for i even:

$$\begin{aligned}\epsilon\psi_{2j-1} + A_j\psi_{2j} + \psi_{2j-2} &= 0\\ A_j^\star\psi_{2j-1} + \epsilon\psi_{2j} + \psi_{2j+1} &= 0\end{aligned} \qquad (8)$$

where $\epsilon = E/t$ with E the energy. There are now two Harper's equations for the hexagonal lattice, in contrast to the single Harper's equation for the square lattice. After some manipulation we find, in a transfer matrix formalism:

$$\begin{pmatrix}\psi_{2j+1}\\ \psi_{2j}\end{pmatrix} = \frac{1}{A_j}\tilde{M}_j\begin{pmatrix}\psi_{2j-1}\\ \psi_{2j-2}\end{pmatrix} \qquad (9)$$

with

$$\tilde{M}_j = \begin{pmatrix}\epsilon^2 - A_jA_j^\star & \epsilon\\ -\epsilon & -1\end{pmatrix}. \qquad (10)$$

As opposed to the transfer matrix for the square lattice, which hops by one site and is linear in energy [8], the graphene transfer matrix hops by two sites and is quadratic in energy. This reflects the lattice periodicity. Since $\tilde{M}_{j+q} = \tilde{M}_j$, the periodicity of the energy spectrum is q. We can now define the transfer matrix over the magnetic unit cell:

$$M(\epsilon) = \begin{pmatrix}M_{11}(\epsilon) & M_{12}(\epsilon)\\ M_{21}(\epsilon) & M_{22}(\epsilon)\end{pmatrix} \equiv \tilde{M}_q\tilde{M}_{q-1}\ldots\tilde{M}_1. \qquad (11)$$

By induction we find that M_{11} is a polynomial of order $(\epsilon^2)^q$, M_{12} and M_{21} are of the form $\epsilon\times(\epsilon^2)^{q-1}$, while M_{22} is a polynomial of order $(\epsilon^2)^{q-1}$. These polynomials have coefficients which depend on k and the magnetic flux. We pick our sample of order $L_y = 2ql$, commensurate with the magnetic unit cell, where l is a large integer and the factor of 2 is added because we will require periodic conditions $\psi_{L_y} = \psi_0$, hence $L_y \equiv 0 \equiv even$. The transfer matrix across the length of this sample is M^l. From Hatsugai [8] we know that the important polynomial to consider is

$$[M^l]_{21}(\epsilon) = 0. \qquad (12)$$

The entire spectrum of energy levels for each k value comes from the zeros of this polynomial of which there are $L_x - 1$. Some of these states are bulk states and others are edge states. We will now characterize the edge and bulk states (bands).

It is easy to find one solution to Eq. (12). Simply take $M_{21}(\epsilon) = 0$ and this will imply that Eq. (12) is satisfied since all upper-triangular matrices remain so when multiplied by another upper-triangular matrix. Hatsugai argues [8] that the energies of the *edge states* are given by the zeros of exactly this polynomial: $M_{21}(\epsilon) = 0$. Since $M_{21}(\epsilon) \sim \epsilon\times(a(\epsilon^2)^{q-1} + b(\epsilon^2)^{q-2} + \cdots)$, there is always one $\epsilon = 0$ solution (zero mode edge state) which does not disperse and $2(q-1)$ non-zero energy solutions (edge-states) which come in pairs: $-\mu_{q-1} \le -\mu_{q-2} \le \cdots \le -\mu_1 \le 0 \le \mu_1 \le \cdots \le \mu_{q-2} \le \mu_{q-1}$. Depending on whether $M_{11}(\mu_i)/|A_q\cdots A_1|$ is $<$, $>$, or $=1$ the edge state will be localized on the left edge, right edge, or be degenerate with the bulk *i.e.* touching a bulk state [8].

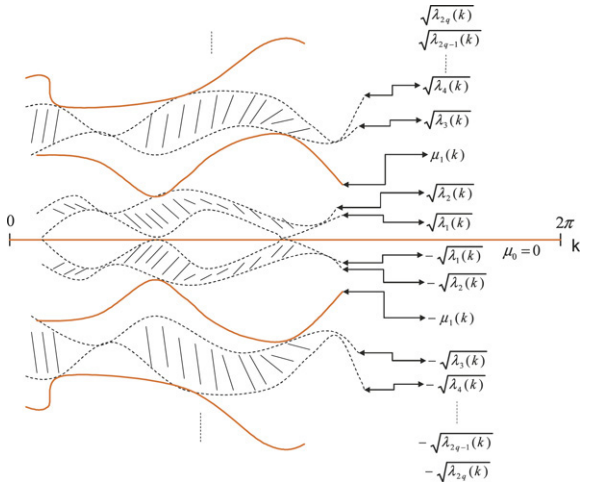

Fig. 3. Schematic plot of the bulk bandstructure and edge states obtained from the transfer matrix formalism. Edge states are solid lines while bulk bands are denoted by the shaded areas bounded by dash and dotted lines.

The bulk states are obtained from the lattice periodicity $j \to j+q$ and the Bloch condition:

$$\begin{pmatrix} \psi_{2q+1} \\ \psi_{2q} \end{pmatrix} = \rho(\epsilon) \begin{pmatrix} \psi_1 \\ \psi_0 \end{pmatrix} \tag{13}$$

with $\rho(\epsilon)$ a pure phase, *i.e.*, $|\rho(\epsilon)| = 1$. We also note that we have the transfer matrix equation

$$\begin{pmatrix} \psi_{2q+1} \\ \psi_{2q} \end{pmatrix} = \frac{1}{A_q A_{q-1} \cdots A_1} M \begin{pmatrix} \psi_1 \\ \psi_0 \end{pmatrix}. \tag{14}$$

Therefore, combining these two, $\rho(\epsilon)$ is an eigenvalue of the 2×2 transfer matrix

$$\rho^{\pm} = \frac{1}{2A_q \dots A_1} \left[\mathrm{Tr}\, M \pm \sqrt{(\mathrm{Tr}\, M)^2 - 4|A_q \dots A_1|^2} \right] \tag{15}$$

where we have used $\mathrm{Det}[M] = \mathrm{Det}[M_q] \dots \mathrm{Det}[M_1] = |A_q \dots A_1|^2$. It is easy to see that the Bloch condition $|\rho(\epsilon)|^2 = 1$ is satisfied for $(\mathrm{Tr}\, M)^2 - 4|A_q \dots A_1|^2 < 0$, based on the fact that $\rho^+ \rho^- = 1$. Since M_{11} and M_{22} are both polynomials of order q in ϵ^2 the solutions are again paired. Let us rewrite

$$(\mathrm{Tr}\, M(\epsilon^2))^2 - 4|A_q \dots A_1|^2 = \prod_{i=1}^{2q} (\epsilon^2 - \lambda_i), \tag{16}$$

with $0 < \lambda_1 \le \lambda_2 \le \cdots \le \lambda_{2q}$. The energy bands are thus

$$\begin{cases} \lambda_{2j+1} \le \epsilon^2 \le \lambda_{2j+2} & \text{bulk state} \\ \lambda_{2j} \le \epsilon^2 \le \lambda_{2j+1} & \text{gap region} \end{cases} \tag{17}$$

for $j = 0, 1, \dots, q-1$ and $\lambda_0 = 0$. The edge states lie in the gap region of the bulk bandstructure and the μ's are given by

$$\mu_j \in [\lambda_{2j}, \lambda_{2j+1}] \quad j = 1, \dots, q-1. \tag{18}$$

We hence have $2q$ energy bands bounded by $4q$ λ's, there are $2q-1$ gaps and $2q-1$ edge states as in Fig. 3. See Ref. [12] for other exact details and examples of the spectrum that can be extracted from this formalism.

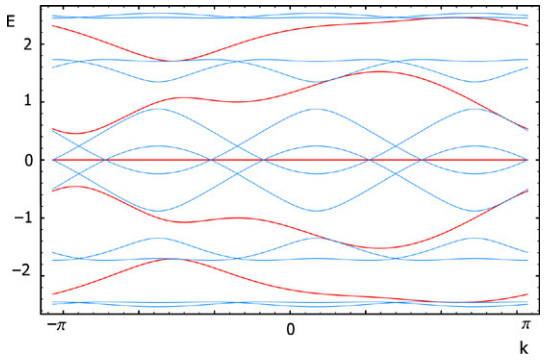

Fig. 4. Edge state and bandstructure configuration for $q = 3$ from transfer matrix formalism. Energy for this and all subsequent figures are in units of the hopping t. Bulk band edges are in blue, edge states in red. (For interpretation of the references to colour in this figure legend, the reader is referred to the web version of this article.)

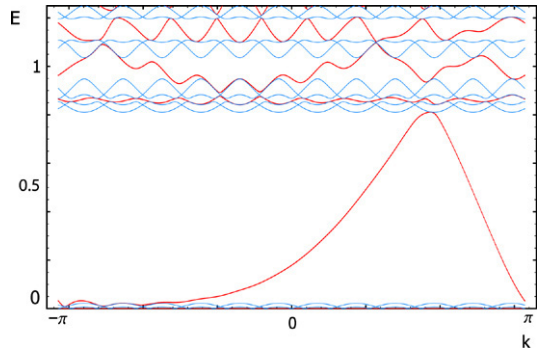

Fig. 5. Edge state and bandstructure configuration for $q = 12$.

3. Edge states and Hall conductance

The Hall conductance in graphene is defined, as usual, as the number of times the edge state wraps around the gap between neighboring energy bands. The number of left (or right) edge states that traverse the entire way across the gap is the Hall conductance in units of e^2/h. We consider the evolution of the bands and edge states as the magnetic field is varied from very strong to weak. We solve for the zeros of the characteristic polynomials $M_{21}(\mu_i) = 0$ and $(\mathrm{Tr}\, M(\lambda_i^{g,b})) \pm 2|A_q \dots A_1| = 0$ introduced in the previous section. In this section we plot only the $\epsilon \ge 0$ states, the negative energy states are a mirror image because of particle–hole symmetry. We also quote the integer Hall conductances in units of $2e^2/h$.

We start with $q = 3$ in Fig. 4 which we characterized analytically in Ref. [12]. We see that the Hall conductance has magnitude unity for a Fermi level in either the first or second gap, clearly in contradiction with the experiments (and the continuum model) which would give $\sigma_{xy} = 1$ or 3 for each gap, respectively.

One crucial observation to notice is that, as we increase q (decrease the magnetic field), the second and third bulk bands become closer and closer together in energy; the gap between them becomes smaller and smaller over the whole Brillouin zone. Eventually the second and third bands move entirely together upon increasing q (lowering B). In Fig. 5 the second and third bands are nearly colliding, but an edge state can still

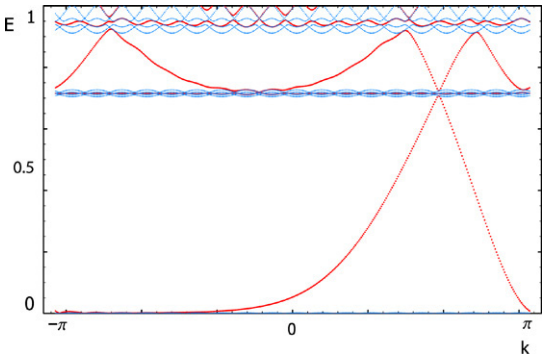

Fig. 6. Edge state and bandstructure configuration for $q = 19$.

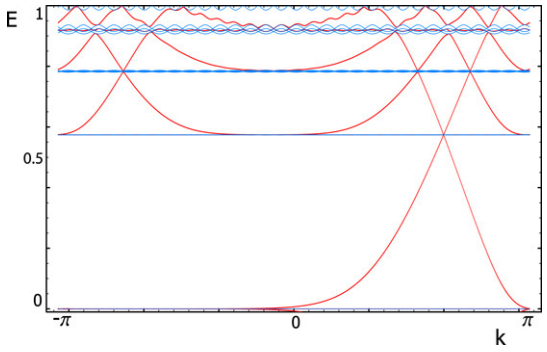

Fig. 7. Edge state and bandstructure configuration for $q = 31$.

be distinguished between them. The gap between the third and fourth band produces Hall conductivity $\sigma_{xy} = 3$. It is this gap which will eventually provide the $\sigma_{xy} = 3$ plateau at lower fields. For $q \geq 12$, one cannot distinguish between the second and third band (nor can one distinguish the edge states between these bands). The second and third band have "collapsed" into a new band, a process which we call "band collapse". After these bands have collapsed there are only distinguishable gaps between the first band and the combined band, and then between the combined band and the fourth band. For $q = 12$ if we then look at the next gap, this again does not match the experiment, since the edge states wind around the gap eight times.

By increasing q even further, we see that the fourth and fifth bands collapse in a similar fashion, and the gap between them vanishes uniformly across the k spectrum as they become a single new band. This happens around $q = 22$. The edge states between the collapsed second and third bands and the collapsed fourth and fifth bands remain the same as before, giving $\sigma_{xy} = 3$ but now the edge states between the collapsed fourth and fifth bands and the sixth band give $\sigma_{xy} = 5$. This process repeats itself while q is increased. The total number of bands increases when q is increased. We show the Landau level bandstructure for $q = 19$ in Fig. 6 and $q = 31$ in Fig. 7. Upon increasing q further, the band collapse produces the odd-integer QHE when the Fermi level is in a gap between the bands which have combined together. Each Landau level at low-filling combines with a partner band *except* the zero mode. This is essential in getting the odd-integer effect. Thus, the experimental situation is obtained as the weak field limit of graphene.

By examining the common properties of the full bandstructure plot for $q = 19$ in Fig. 8 it appears that the spectrum of bands and edge-states can be classified into two parts: a relativistic section and a non-relativistic section. This structure originates from the original tight-binding dispersion relations without the B field,

$$\epsilon(k_x, k_y) = \pm t\sqrt{1 + 4\cos^2\frac{\sqrt{3}}{2}k_x + 4\cos\frac{\sqrt{3}}{2}k_x\cos\frac{3}{2}k_y}. \quad (19)$$

The Dirac nodes are located at $(\pm\frac{4\pi}{3\sqrt{3}}, 0)$ and $(\pm\frac{2\pi}{3\sqrt{3}}, \pm\frac{2\pi}{3})$. The linearized dispersion relations persist up to around $E \approx$

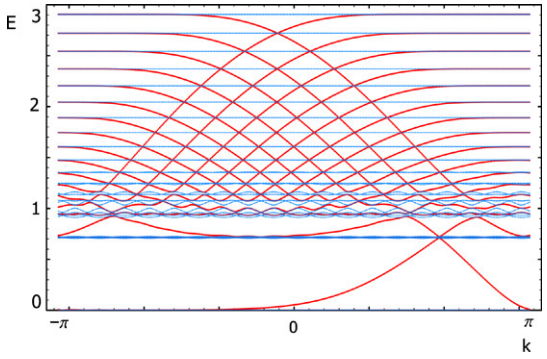

Fig. 8. Edge state and bandstructure configuration for $q = 19$ and for the entire $\epsilon > 0$ spectrum. This shows the relativistic (low-energy) to non-relativistic (high-energy) crossover which occurs around $\epsilon \sim 1$.

t (≡1). Above this energy scale the bands become parabolic. Accordingly, in Fig. 8, $\sigma_{xy} = 1, 3$ at low energy and the energy of bulk levels goes as $E_n \approx \sqrt{n}$, a feature of relativistic Landau levels. On the other hand starting from the top of the bands (where parabolic bandstructure is expected) there is almost equal spacing between each of these Landau levels, which is a feature of the harmonic-oscillator-like non-relativistic Landau levels. A σ_{xy} of magnitude 1 is seen in the first gap from the band ceiling and the magnitude increases by one for each Landau level below the top. A similar thing occurs for the non-relativistic levels near the bottom of the set of bands. The crossover region is at $E \approx t$, which is the energy scale of the hopping parameter and where the band collapse occurs.

The odd-integer sequence shown in Fig. 7 is clearly represented in the experimental data which, as stated before, is in the "low" magnetic field limit of graphene. With a flux $\phi = 1/q$ in each unit cell the magnetic field is $\sim\frac{7.8\times10^4}{q}$ Tesla which is very large for the q-values we considered. For the highest experimentally realizable magnetic fields we would expect $q \sim 1300$ and the odd-integer sequence would be continued to larger values. Abnormalities in this sequence would not arise until many more Landau levels were filled. Overall, there will be a sequence of odd-integer quantum Hall conductances followed by a crossover regime in the region $E \sim t$. This leads to a relativistic-non-relativistic crossover where the Landau level spacings change character from $n^{1/2}$ to n. The non-relativistic energy levels will then persist to higher energies.

3.1. Semenoff mass and Zeeman terms

The previous formalism can be easily extended to incorporate the case of a non-zero Semenoff mass m. As an example, for Boron Nitride (BN) the hamiltonian has the form

$$H = -t\sum_j((c^\dagger_{2j-1}c_{2j}A_j + c^\dagger_{2j}c_{2j+1} + h.c.) + m(c^\dagger_{2j-1}c_{2j-1} - c^\dagger_{2j}c_{2j})). \quad (20)$$

The new Harper's equations are

$$(\epsilon + m)\psi_{2j-1} + A_j\psi_{2j} + \psi_{2j-2} = 0$$
$$A^\star_j\psi_{2j-1} + (\epsilon - m)\psi_{2j} + \psi_{2j+1} = 0 \quad (21)$$

and the transfer matrix now becomes

$$\tilde{M}_j = \begin{pmatrix} \epsilon^2 - m^2 - A_jA^\star_j & \epsilon - m \\ -(\epsilon + m) & -1 \end{pmatrix}. \quad (22)$$

As we can see, $\tilde{M}_q\tilde{M}_{q-1}\ldots\tilde{M}_1 = (\epsilon+m)\times P^{(q-1)}(\epsilon^2)$ where $P^{(q-1)}(\epsilon^2)$ is a polynomial of order $q-1$ in ϵ^2. Hence, the former zero energy edge state has now moved to $\mu_0 = -m$. There are no edge states between $[-|m|, +|m|]$, but the rest of the analysis applies. We plot the bandstructure for $m = 0.1$, $q = 19$ (see Fig. 9(a)).

In order to include the Zeeman term we can calculate the bandstructure from two separate transfer matrix polynomial equations and combine the solutions. These two transfer matrices correspond to spin up and spin down and are given by

$$\tilde{M}_{j\pm} = \begin{pmatrix} (\epsilon \pm \Delta\epsilon_z)^2 - A_jA^\star_j & (\epsilon \pm \Delta\epsilon_z) \\ -(\epsilon \pm \Delta\epsilon_z) & -1 \end{pmatrix} \quad (23)$$

where $\Delta\epsilon_z$ is the Zeeman energy splitting. The bandstructure for $q = 19$ and small Zeeman splitting is plotted in Fig. 9(b). We can trivially extend these results to include the effects of combined Semenoff mass and Zeeman splitting by using the following two transfer matrices:

$$\tilde{M}_{j\pm} = \begin{pmatrix} (\epsilon \pm \Delta\epsilon_z)^2 - m^2 - A_jA^\star_j & (\epsilon \pm \Delta\epsilon_z - m) \\ -(\epsilon \pm \Delta\epsilon_z + m) & -1 \end{pmatrix}. \quad (24)$$

The bandstructure for the combined Semenoff and Zeeman splittings is shown in Fig. 9(c) where $\Delta\epsilon_z > m$ which is the expected experimental situation.

We now focus on the breaking of spin and/or valley degeneracy only in the $n = 0$ Landau Level. The idea of spin splitting is very natural since $g \sim 2$ in graphene and there is a large magnetic field applied perpendicular to the sample. Splitting the valleys, however, is more subtle since there is no natural alternating sublattice potential or applied strain. The valley splitting most likely arises at the interaction level but the effect of valley splitting on the quantum Hall conductances can be tested through the single-particle Semenoff mass. We investigate the expected changes to the QHE plateau structure and edge states when these splittings can be resolved energetically.

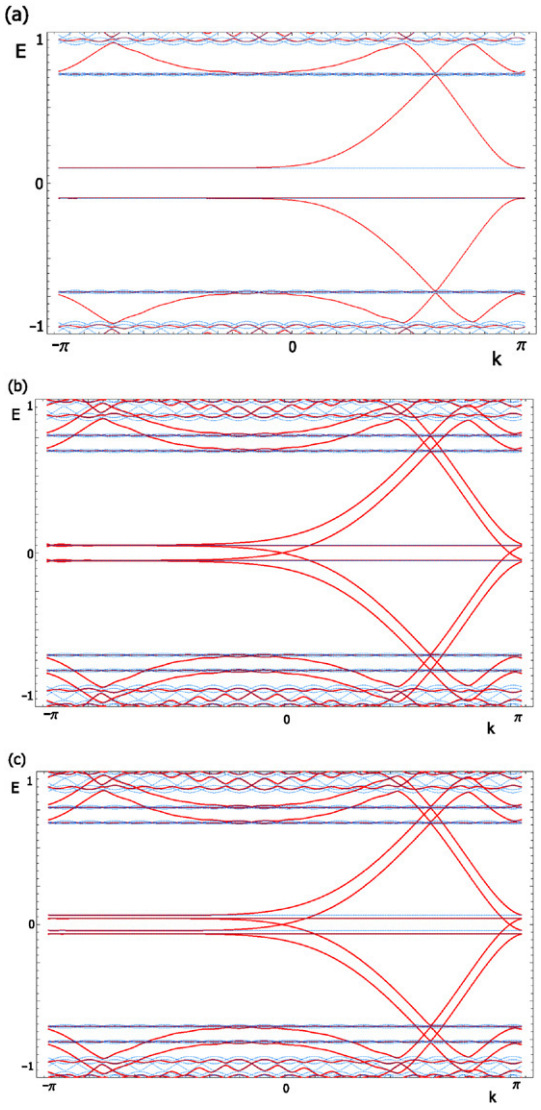

Fig. 9. Landau level bands and edge states around $E = 0$ for: (a) valley splitting only; (b) spin splitting only; (c) spin and valley splitting. Note that in (b), (c) there are edge states inside the central gap. These are only here if there is spin splitting.

First we consider the case where only the valleys are split in the $n = 0$ level. As stated above this is very similar to the case of a non-zero Semenoff mass and the bandstructure can be seen in Fig. 9(a). There is a gap at zero energy leading to an additional zero conductance plateau, however here there are no edge states in the gap. The Hall conductances around zero energy are $\sigma_{xy} = -2, 0, 2$ in units of e^2/h.

Next is the case of only spin splitting. Due to the Zeeman effect the spin states in each Landau level will be split by $g\mu_B B$. For the $n = 0$ Landau level one spin state is pushed above zero energy and the other is pushed below zero energy. When the chemical potential lies in the gap at zero energy between the split spin states there is an additional quantum Hall plateau with $\sigma_{xy} = 0$. This leads to the same Hall conductance sequence as the Semenoff mass. The picture is not quite this simple because this gap, unlike the Semenoff mass gap discussed above, contains edge states which can be seen

in Fig. 9(b). Usually the presence of edge states in the gap signals a non-zero quantum Hall conductance but here there is actually one electron edge state and one hole edge state. These two edge states combine together to give zero Hall conductance but produce a non-zero spin-Hall conductivity since they are spin-polarized in opposite directions:

$$\sigma_{\text{spin}} = 2\frac{e^2}{\hbar}. \tag{25}$$

This spin current can be observed in a 4-terminal geometry or in a system with magnetic leads. These edge states were first predicted in Ref. [13].

Finally we come to the case where there are both spin and valley splittings. The Fermi level lies in a gap when the $n = 0$ level is unfilled, 1/4-filled, 1/2-filled, 3/4-filled, and completely filled yielding a sequence of quantum Hall conductances $\sigma_{xy} = -2, -1, 0, 1, 2$ in units of e^2/h when the chemical potential lies in each of these gaps respectively. The band picture with each of these conductances can be seen in Fig. 9(c). This sequence matches the data recently produced in Ref. [14] in very high magnetic fields.

4. Conclusion

We have shown that the "relativistic" QHE in graphene has its origin in a band-collapse picture where two bands become degenerate upon decreasing the flux per plaquette. A series of exact results for the honeycomb lattice have been given, as well as an index theorem for the number of dirac modes in a magnetic field. At large magnetic fields, the system has a transition between "relativistic" and non-relativistic QHE. When the spin-gap is resolved, the system exhibits a spin-Hall effect due to existence of opposite spin electron and hole edge states in the gap. We discussed the effects of disorder and adding a Semenoff mass term. We concluded with discussion on spin and valley splitting in the $n = 0$ Landau level and its implications for the QHE.

Note: After the completion of this work we noticed there is some overlap with the recent work in Ref. [15]. Where the works overlap they agree on the conclusions.

Acknowledgements

B.A.B. acknowledges support from the SGF. T.L.H. acknowledges support from NSF. This work is supported by the NSF under grant numbers DMR-0342832 and the US department of Energy, Office of Basic Energy Sciences under contract DE-AC03-76SF00515.

References

[1] K.S. Novoselov, et al., Nature 438 (2005) 197.
[2] Y. Zhang, et al., Nature 438 (2005) 201.
[3] R. Jackiw, C. Rebbi, Phys. Rev. D 13 (1976) 3398.
[4] A.M. Schakel, Phys. Rev. D 43 (1991) 1428.
[5] N.M.R. Peres, F. Guinea, A.H.C. Neto, Phys. Rev. B 73 (2006) 125411.
[6] V.P. Gusynin, S.G. Sharapov, Phys. Rev. Lett. 95 (2005) 146801.
[7] Y. Hatsugai, M. Kohmoto, Y.-S. Wu, Phys. Rev. B 54 (1996) 4898.
[8] Y. Hatsugai, Phys. Rev. B 48 (1993) 11851.
[9] G.W. Semenoff, Phys. Rev. Lett. 53 (1984) 2449.
[10] F.D.M. Haldane, Phys. Rev. Lett. 61 (1988) 2015.
[11] A. Abouelsaood, Phys. Rev. Lett. 54 (1985) 1973.
[12] B.A. Bernevig, T.L. Hughes, S.C. Zhang, Inernat. J. Modern Phys. B 20 (2006) 3257.
[13] D.A. Abanin, P.A. Lee, L.S. Levitov, Phys. Rev. Lett. 96 (2006) 176803.
[14] Y. Zhang, et al., Phys. Rev. Lett. 96 (2006) 136806.
[15] Y. Hatsugai, T. Fukui, H. Aoki, Phys. Rev. B 74 (2006) 205414.